

A Unified Stochastic Mechanism Underlying Collective Behavior in Ants, Physical Systems, and Robotic Swarms

Lianhao Yin ^{1*}, Haiping Yu ², Pascal Spino ¹ Daniela Rus ¹

¹ Computer Science and Artificial Intelligence Laboratory, MIT, MA, US

² The International Institute for Industrial Environmental Economics, Lund University, Sweden

*E-mail: lianhao, spino, rus@csail.mit.edu, haiping.h.yu@gmail.com

Biological swarms, such as ant colonies, achieve collective goals through decentralized and stochastic individual behaviors. Similarly, physical systems composed of gases, liquids, and solids exhibit random particle motion governed by entropy maximization, yet do not achieve collective objectives. Despite this analogy, no unified framework exists to explain the stochastic behavior in both biological and physical systems. Here, we present empirical evidence from *Formica polyctena* ants that reveals a shared statistical mechanism underlying both systems: maximization under different energy function constraints. We further demonstrate that robotic swarms governed by this principle can exhibit scalable, decentralized cooperation, mimicking physical phase-like behaviors with minimal individual computation. These findings established a unified stochastic model linking biological, physical, and robotic swarms, offering a scalable principle for designing robust and intelligent swarm robotics.

1 Introduction

Biological swarms, such as ant colonies, exhibit seemingly random individual actions during foraging, object transport, and colony migration, while the collective swarm achieves intelligent behavior. In contrast, individual physical particles in gases, liquids, and solids also move randomly, but collectively they do not pursue a common goal driven by intrinsic motivation—such as transporting objects or moving in a preferential direction. Instead, matter particles exhibit collective physical properties such as phase, temperature, and pressure. Noise provides several important benefits to collective systems. It can facilitate alignment in locust swarms (1), induce transitions between disordered and ordered phases in mobile insect groups (2), and enhance global human coordination in network experiments (3). To date, no unified principle exists to explain the stochastic behavior observed in both systems. In general, in biological swarms, various simplified physical models have been proposed to explain collective behaviors, for example, the Ising model for cooperative transport (4), the Vicsek model to describe the flocking of birds (5), the dynamic model for bacteria turbulence (6) and human panic escape (7), and the quantification of collective state (8). Algorithmic approaches have also been used to model flocking and swarming, incorporating gradient, consensus, and group objective terms (9), as well as neural network models such as the ring attractor network to explain order formation in locust swarms (10). Specifically, several modeling methods have been employed to represent noise and investigate its role in swarms. A simple approach is to add white noise to the action (11). Another approach introduces stochastic behavior by random sampling of peer perception (12). In addition, Brownian motion has been incorporated into differential equations to model alignment dynamics (13). However, these models often impose external coordination or lack a unified explanation for stochasticity across both physical and biological domains. Inspired by D’Arcy Thompson’s view that scientific understanding often arises from identifying

analogies rather than causalities (14), our goal is not to reduce biological behavior to physical mechanics, but rather to uncover a shared principle underlying both.

Therefore, one of the motivations of the paper is to understand the distribution randomness of biological swarms in constrained environments through tracking the motion of ants in a constrained environment, and to explore the randomness in multi-robot systems in which each robot is considered as a particle to find a relation to randomness in physical particles.

Current multi-robot systems require communication to each other and a central controller to achieve collective goal or behavior, for example, formation control (15), self-reproduction (16), and moving an object using particle robots (17). When the number of robots increases, the speed and ability of the system to achieve the collective goal, e.g. moving an object, decrease (17). This is due to that the demands for accurate coordination and consensus increase (18, 19) in compromise of robustness. The programming of centralized, multi-robot systems for various tasks is also difficult due to the complexity of algorithmic and mechanical coordination between units (19, 20). However, experimental robotic swarms such as manorobots (21), ant-like robots (15), magnetic-driven microrobots (22), and granular matter controlled by the magnetic field (23) instead utilize a fully decentralized control approach with minimum individual computation to allow scaling to larger numbers of robots with higher collective capabilities. Therefore, the second motivation of this paper is to replicate the stochastic action of ant swarms, enabling a fully decentralized and scalable robot swarm to achieve a common goal while necessitating minimum computation by each individual robot.

2 Ant swarm experiments

To investigate stochastic behavior in the ant swarm, we measured the speed and steering angle of biological ants (*Formica polyctena*, one of the *Formica* species) in a constrained environment. *Formica polyctena* has been shown to sense both pheromone and colored light to navigate to

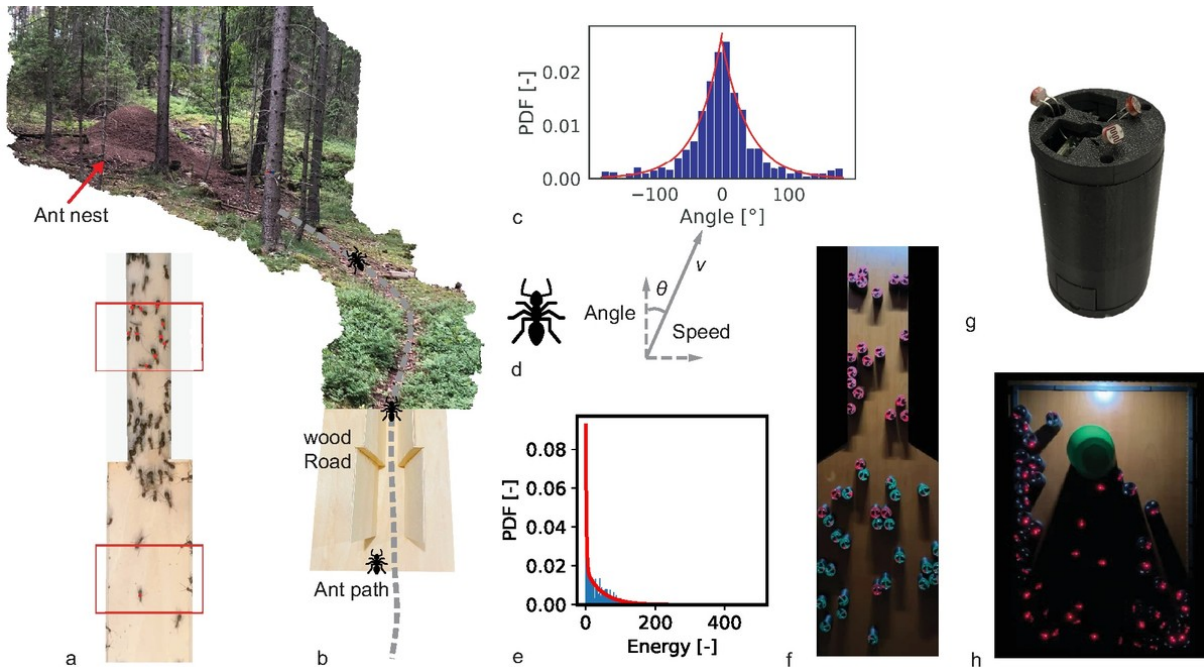


Figure 1: (a) We track the ants on the up and low side of the wood road, which is marked by red squares. (b) We put the wood road on the ant path between the ant nest and the forage areas. (c) The probability density of the angle rate of the ant. The red is fitted with an exponential distribution. (d) Illustrate how the speed and angle are defined. (e) The probability density function of energy of an ant, which is defined as $(E = \frac{1}{2}mv^2)$, where m, v are the mass and speed of the ant, respectively. (f) The setting of robotic experiments for narrow road crossing. (g) Illustration of the robot hardware. (h) The setting of robotic experiments for moving object.

the nest (24). A wooden road was constructed (Fig. 7) and placed within the natural flow path of the ant that leads to the nest (Fig. 1) serving as the main study location. This area has the highest density of ants in traffic. A top-down camera was used to record the ant flow (Fig. 1). The wooden road was placed within the ant nest to ensure a homogeneous pheromone coating on its surface prior to experiments. The length of the wooden road was chosen to maintain uninterrupted ant flow. The width of the road matched the original flow path to preserve natural traffic conditions and prevent ants from entering other paths. Previous experiment with different ant species show that the bidirectional ratio of the ant flow does not significantly influence the flow rate and the crowdedness of ants in congestion (25). Accordingly, our experiments did not

treat the bidirectional ratio as an experimental variable.

3 The stochastic behaviour in ant swarm

The analysis of individual ant trajectories, based on the tracking method described in Section 7.2, shows that both the energy distribution ($E = \frac{v^2}{2}$, where v is the speed) and the distribution of the steering angle rate (θ) follow exponential forms consistent with energy-based statistical models. Specifically, the probability density function of energy takes the form $p(v_i^2) = \phi \frac{1}{kT_1} e^{-\frac{1}{kT_1} v_i^2} + (1 - \phi) \frac{1}{kT_2} e^{-\frac{1}{kT_2} v_i^2}$, and that of the steering angle rate takes the form $p(\theta) = \frac{1}{kT_\theta(v)} e^{-\frac{1}{kT_\theta(v)} \theta}$ (Fig. 1c,e).

The speed distribution of the ants follows a bimodal exponential form, analogous to the gas and liquid phases in thermodynamic systems (Fig. 2a-h). The phase with low temperature resembles a liquid state and the phase with high temperature resembles a gas-like state. The KS statistic for a single-phase fit is significantly higher than that for a two-phase fit, indicating a statistically better fit with two distinct energy distributions (Fig. 2j). The proportion of ants associated with the high temperature phase decreases as they enter the narrow road (Fig. 2i), meaning that more ants are in the low temperature phase and the low speed expectation in the narrower part of the road. The high temperature component T_2 contributes more significantly to the average ant flow. Previous work (25) showed that flow rate decreases with increasing ant density. Similarly, the temperature component T_2 in the speed distribution is inversely correlated with swarm density. The distribution of the steering angle rate at each speed also follow an energy-model (Fig. 3a-h). The temperature of the distribution T_θ decreases with the average speed of the ants (Fig. 3i), indicating greater steering variability at low speeds and more constrained steering at higher speeds.

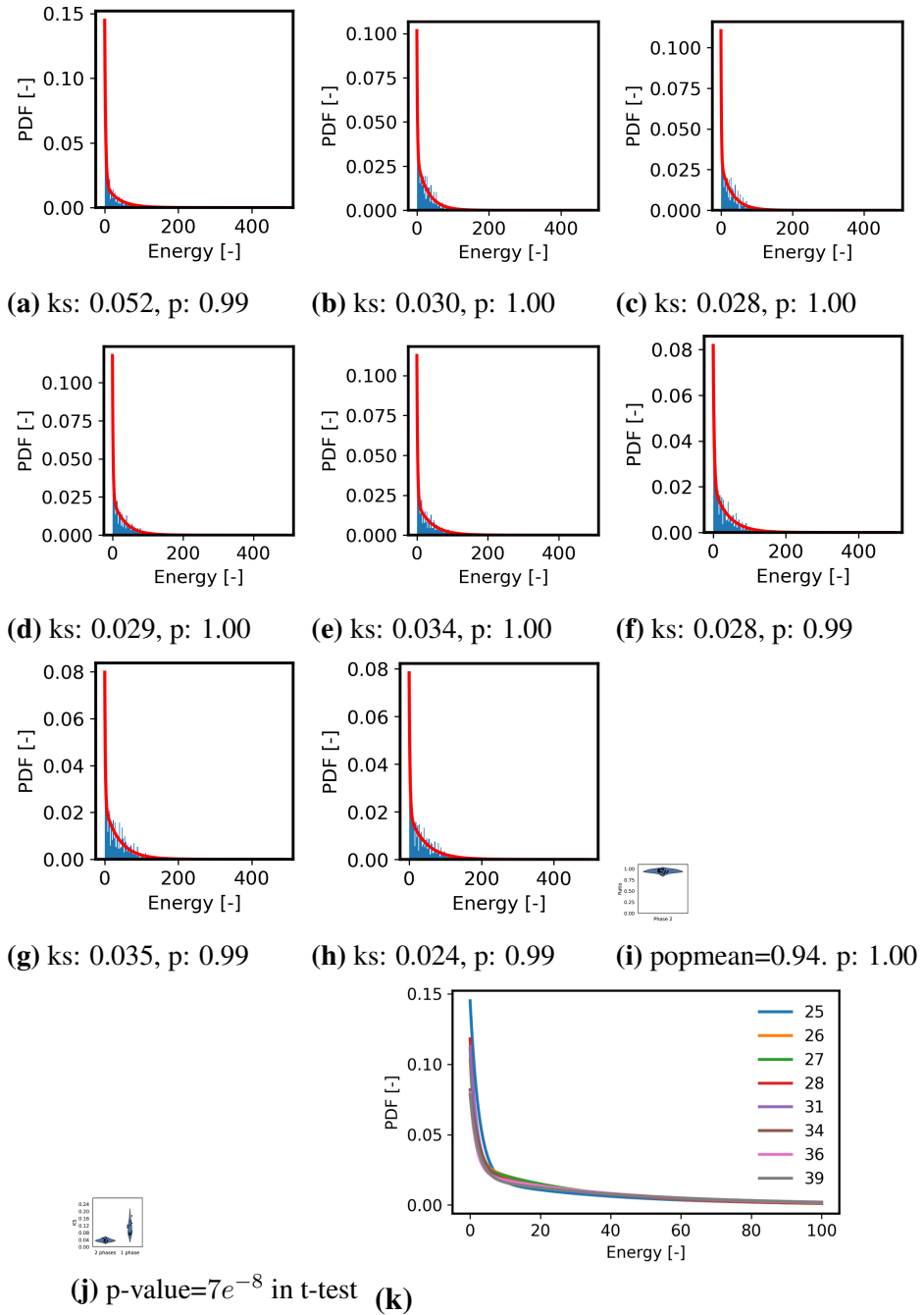


Figure 2: The speed distribution $(p(v_i^2) = \phi \frac{1}{kT_1} e^{-\frac{1}{kT_1} v_i^2} + (1 - \phi) \frac{1}{kT_2} e^{-\frac{1}{kT_2} v_i^2})$ in red). (a-h) Energy level at 25, 26, 27, 28, 31, 34, 36, 39 respectively, (g) Probability density curve at different energy level. Unit: $1/10^{10}$ J, (j) KS of 1 phase versus 2 phases fitting, (i) Ratio of ant at upper and lower side in phase 2

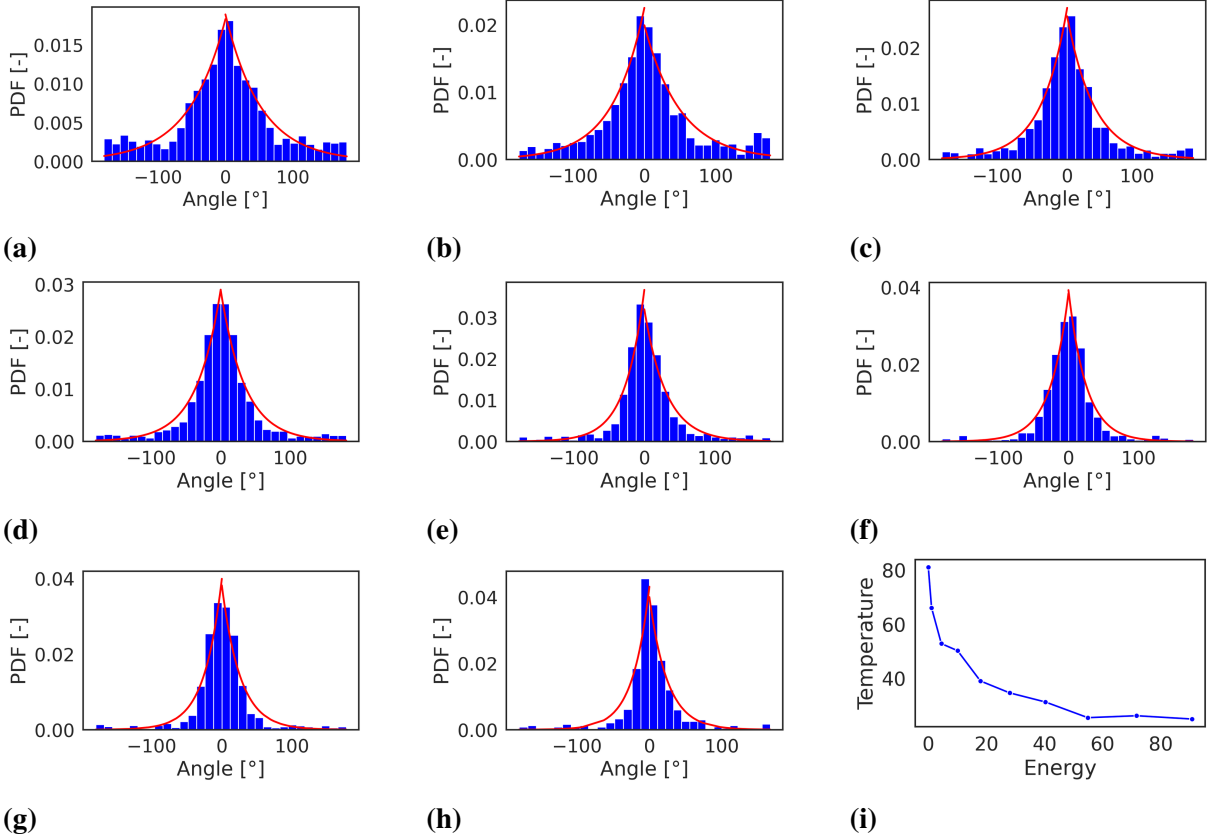


Figure 3: Steering angle rate distribution at different energy level. (a) 4.5 (ks-statistic: 0.060, p-value: 0.3) (b) 10, (ks-statistic: 0.060, p-value: 0.3) (c) 18, (ks-statistic: 0.076, p-value: 0.4) (d) 28, (ks-statistic: 0.076, p-value: 1) (e) 40, (ks-statistic: 0.076, p-value: 1) (f) 54, (ks-statistic: 0.073, p-value: 1) (g) 71, (ks-statistic: 0.10, p-value: 1) (h) 90, (ks-statistic: 0.088, p-value: 1), (i) Temperature of the steering angle rate distribution $p(\theta) = \frac{1}{kT_{\theta}(v)} e^{-\frac{1}{kT_{\theta}(v)}\theta}$ at different energy level, where T is a function energy. Intuitively, the steering angle rate range are wider at low energy and low speed.

4 Robotic experiments: apply stochastic mechanism to robotic swarm decisions

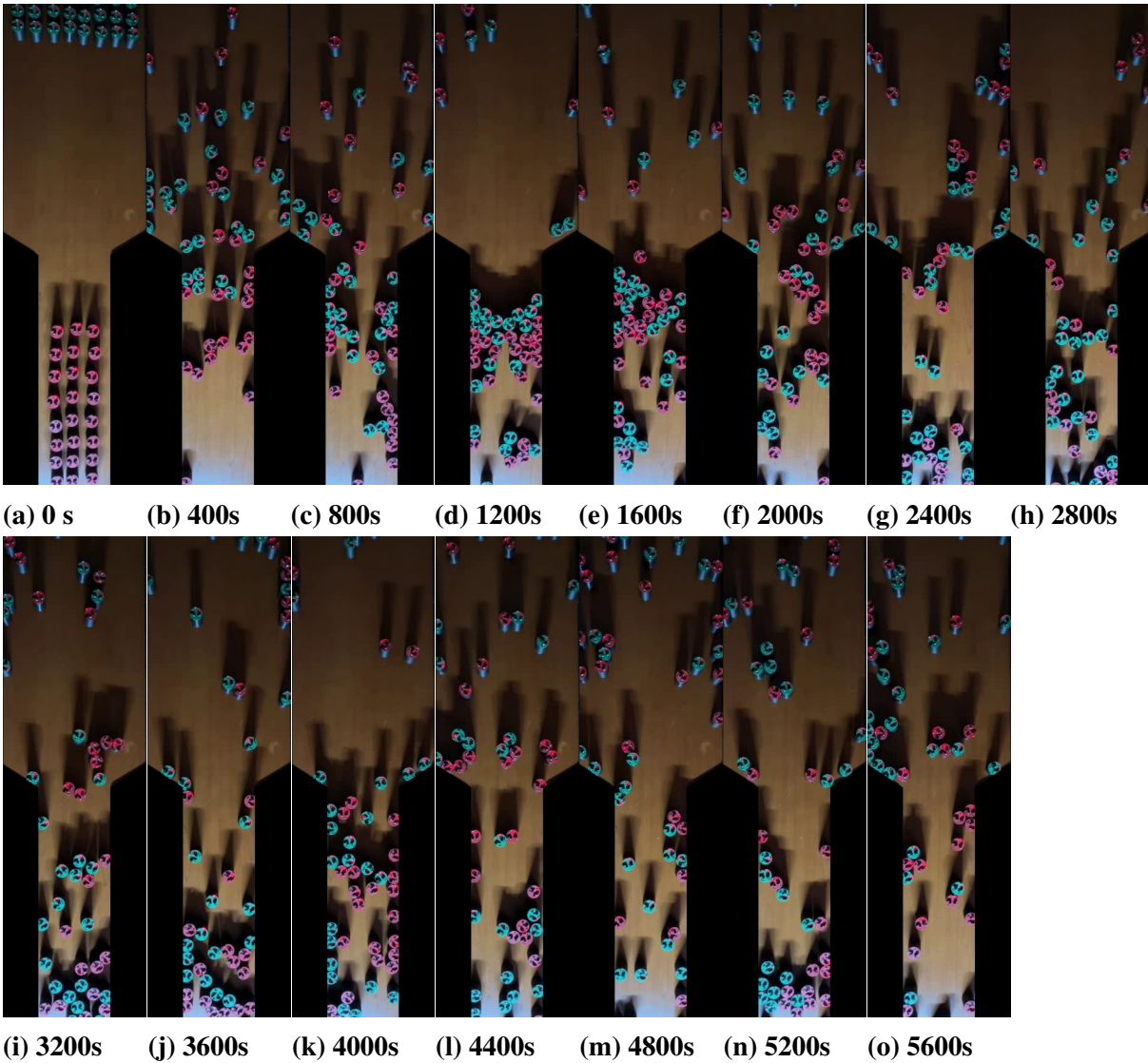


Figure 4: Long time robotic crossing experiments

As the second motivation is to replicate the randomness using the discovered energy model from ants to a robotic swarm to achieve scalable and collective behavior with minimum computation. In this framework, actions such as speed and steering angle are modeled as stochastic

variables governed by energy-based probability distributions.

First, we demonstrate that swarm robots governed by the derived principle (Tab. 1, Alg. 2) exhibit flow behavior consistent with that observed in ant swarms. The road configuration (Fig. 16a) for robot swarm is the same as for the field experiments. Each robot (Fig. 1g), Tab. 2) is equipped with three photoresistors (Fig. 16c) to infer heading direction based on light signals using Alg.1. To maintain a spatial density comparable to that of ant swarms, we adjusted the number of robots accordingly (Sec. 7.5.1). Unlike ants, which can overlap and exhibit compliance in dense environments, our robots are rigid and cannot overlap. As such, we focus on their ability to traverse the narrow road rather than matching the exact flow rate of the biological system.

The robot swarm moves bidirectionally through the narrow road, guided by the energy-based control policy (Alg. 2). There is no communication between each robot, which enables the scalability of the robotic systems. The results (Fig. 4) demonstrate that robots can pass each other and achieve effective collective navigation, mimicking the cooperative behavior of ants in natural environments.

In the second experiment (Fig. 13), a fixed number of robots was placed in a constrained space, where the upper and lower walls could move vertically under the influence of a constant external force. The robots were controlled using Alg. 3. The temperature of the robot swarm was kept constant in each experiment, while the force applied to the walls varied. As shown in Fig. 6w, the observed pressure–volume relationship is analogous to that of an ideal gas. Swarm robots governed by the energy-based control policy exhibit physical behaviors governed by stochastic mechanisms, consistent with the second law of thermodynamics (Alg. 3). This further demonstrates that the unified principle underlying ant swarms and physical particles also governs the behavior of programmed robotic swarms.

In the final experiment, we evaluated whether the proposed principle can support intelli-

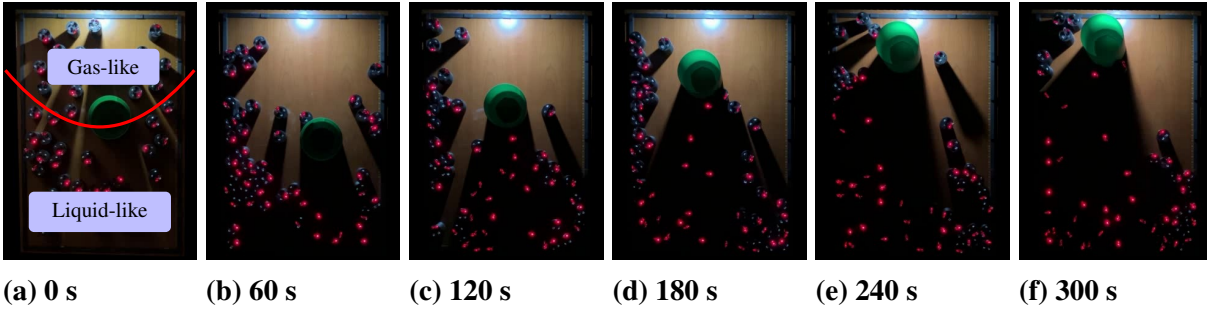


Figure 5: Robots move the green object toward the light sources. Robots in illuminated regions (red LEDs visible) behave in a **gas-like phase**; those in darkness remain in a **liquid-like phase**.

gent behaviors such as object transport, inspired by how ants move objects. We first show that the robots physically connected to the object successfully moved the object toward the goal (Fig. 14) using Alg. 4. Next, we disabled the robots’ physical connection to the object. Each robot followed the same control algorithm, requiring minimal computation based on a temperature function derived from the position of the object and the goal (Alg. 5). The temperature function depends on a single parameter that switches between high and low values based on the local light level. The light levels are high between the object and the target, whereas the area behind the object remains shadowed. This policy (Alg. 5) drives the robot swarm to move the object toward the target (Fig. 5). A clear phase separation emerges within the swarm: robots in dark regions exhibit low temperature and behave like a liquid phase, while those between the object and the light source exhibit high temperature, corresponding to a gas-like phase. (Fig. 5.a, Fig. 6). This experiment shows that the swarm not only performs intelligent object transport but also retains physical characteristics such as phase separation. The performance of the robotic swarm increases with the number of robots (Fig. 6, Fig. 17), while the computational load per robots does not increase and is kept minimum.

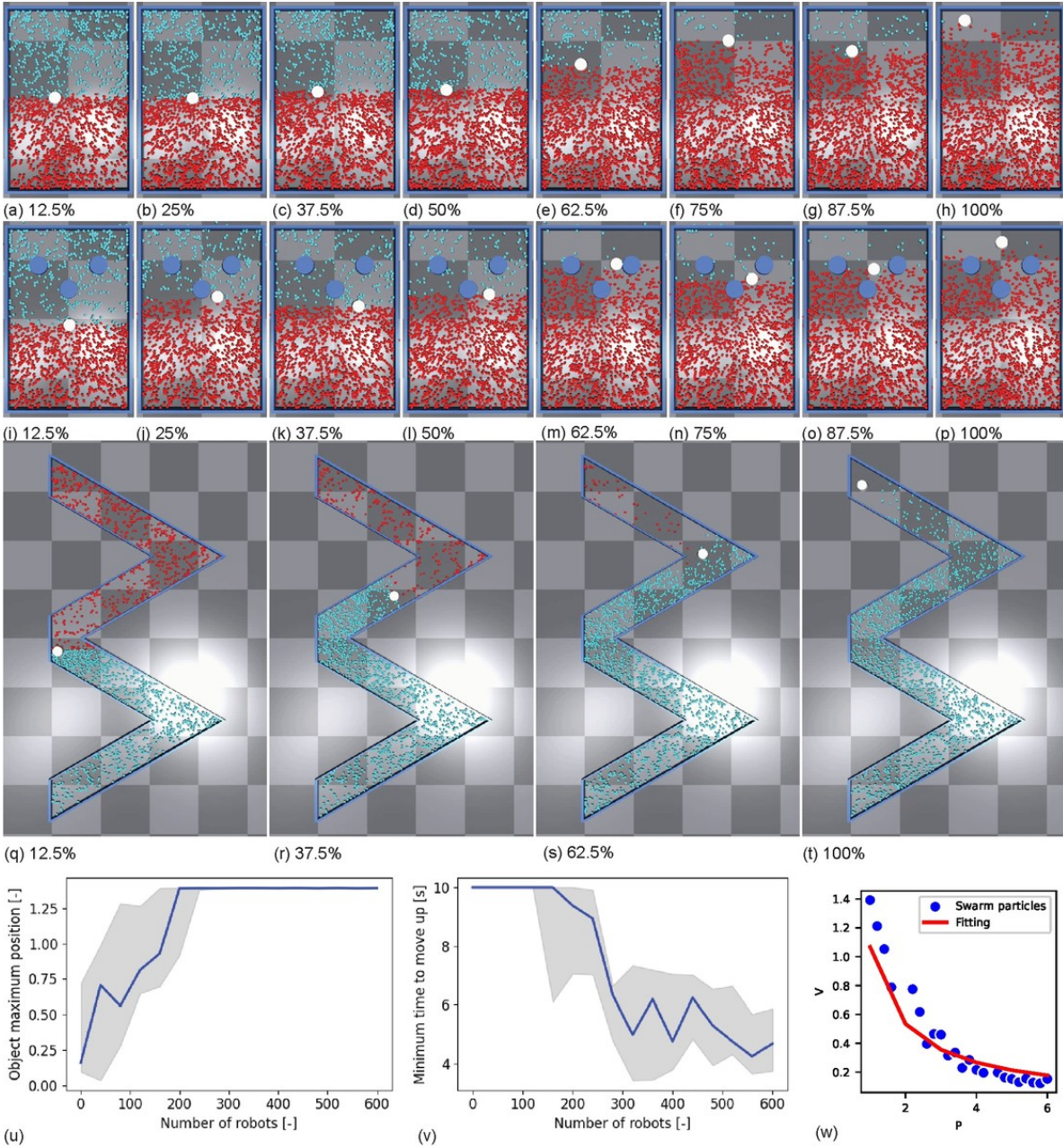


Figure 6: 1200 robots move object without physical connection: (a-h): robot swarm move object without obstacle to the top, (i-p): robot swarm move object with obstacle to the top, (q-t): robot swarm move object zig curve to the top. Capacity quantification of robotic swarms: u) The capacity of robotic swarm quantified by maximum object moving distance, increase with number of robots, (v) The minimum time to move object to desired position, decreases with number of robots. (w) Temperature increases to keep density the same in compression experiments

5 Disucssion

According to the statistical mechanism (Eq. 2, 3), the probability density functions of speed and angle represent closed-form solutions to the entropy maximization problem under energy constraints, with expected energy $E = kT$. Intuitively, the individual actions of the ant, such as speed and steering angle rate, are stochastic and not deterministic, but with a common expectation of speed and steering angle rate.

	Speed	Steering angle rate	Energy (speed)	Energy (angle)
Ants	$p(v^2) = \sum_i^2 \phi_i \frac{1}{E_1} e^{-\frac{1}{E_1} v^2}$ $\sum_i^1 \phi_i = 1$	$p(\theta) = \frac{1}{E(v)} e^{-\frac{1}{E(v)} \theta}$	$E_i, i \in [0, 1]$	$E(v)$
Physical particles	$p(v^2) = \frac{1}{E} e^{-\frac{1}{E} v^2}$	Uniform/Random	$E = kT$	-
Swarm Robots (move)	$p(v^2) = \frac{1}{E(x)} e^{-\frac{1}{E(x)} v^2}$	Uniform/Random	$E(x)$	-
Swarm Robots (cross)	$p(v^2) = \frac{1}{E} e^{-\frac{1}{E} v^2}$	$p(\theta) = \frac{1}{E(v)} e^{-\frac{1}{E(v)} \theta}$	E	$E(v)$

Table 1: Comparison of distribution of speed and steering angle rate of ants, physical particles and robot swarm. The distribution of speed and angle are the closed form solution of entropy maximization (Eq. 2). The main differences are what the probability represents and the energy function in the constraints (Eq. 2). The energy function of speed(v) related to the density of the ant, the energy function of steer angle(θ) of the ants related to the speed. The energy function of physical particles are the system state which can be measured by temperature(T, k is a constant). The energy function of speed (v) of swarm robots in crossing experiments is a constant, and that of steering angle is a function of speed. The energy function of speed (v) of swarm robots in moving object experiments is a function of relative position of the object (x) measured by the lightness.

Table 1 summarizes the speed and steering angle distributions of ants, robots along with those of the physical particles. In the classical Boltzmann distribution (26), physical particle speed, such as that of atoms or molecules, is governed by a single energy component E_1 , since the system is characterized by a single equilibrium temperature. In contrast, the speed distri-

bution of *Formica polyctena* exhibits two energy components, E_1 and E_2 , yet retains the same exponential form of the energy distribution. Although the direction of motion of the bulk particles is typically random or uniformly distributed, the steering angle rate of the ants also follows an energy-based distribution, with the energy $E = kT$ varying as a function of speed (Fig. 3i). The energy function of speed and the steering angle rate in an ant swarm are biologically programmed, whereas the particles in the bulk of a solid, liquid, or gas are governed by energy exchanges. Although the energy model's arguments are different and have different numbers of energy components, the underlying distributions share a common exponential form, which represents a closed form of entropy maximization. Intuitively, the ants maximize the entropy of the speed and steering angle distributions while maintaining constant average values. This provides a unified statistical explanation for the stochastic behavior observed in both ant swarms and physical particles.

6 Conclusion

The energy modeling of The stochastic behavior describes the distribution of individual ant energy in constrained environments and shares the same form as the particle energy distribution in an isolated ideal gas system. This principle enables fully decentralized, robust, and scalable collective robotic systems that do not require communication between units. Robotic swarms governed by this principle exhibit intelligent behaviors, such as object transport, while preserving physical properties such as phase transitions, all in a decentralized fashion. This discovery provides a unified theoretical foundation for describing stochastic behavior across ant swarms, physical particles, and robotic swarms. It bridges the domains of statistical physics, biology, and robotics, offering a framework for designing collective systems with minimal computation per robot. Looking ahead, the energy function, as a closed-form solution to entropy maximization, enables fully decentralized robotic swarm systems with minimal computation and balanced ca-

pability. This approach holds promise for practical applications, ranging from microrobotics in healthcare to large-scale autonomous robotics in warehouses and beyond.

7 Methods

7.1 Biological experimental settings

7.1.1 Biological experimental setup

The dimensions of three roads are illustrated in Fig. 7. The narrow straight road has a wide section 40 mm in width and a narrow section 20 mm wide.

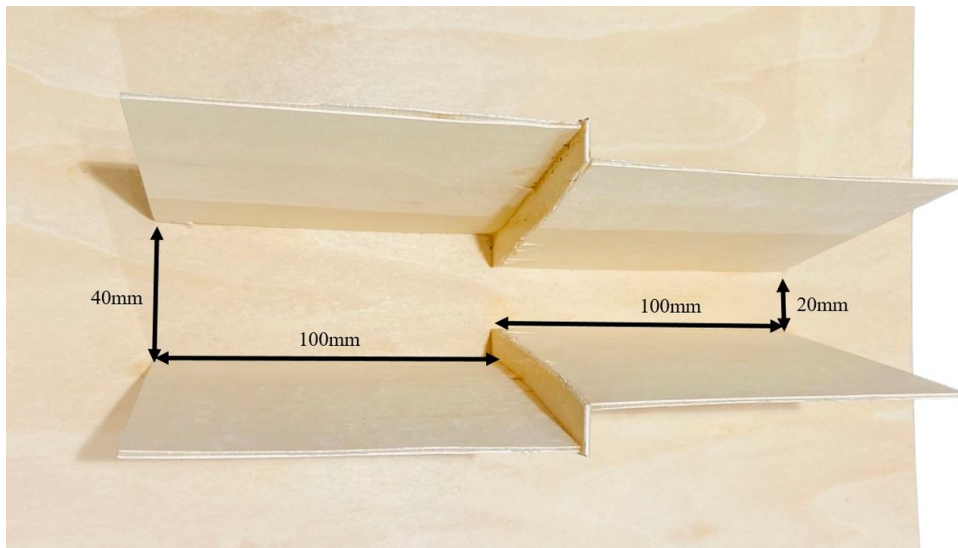


Figure 7: Road dimension

The raw image has height of 1920 and width of 1080 and the images are normalized such that 1mm equals to 3.04 pixels.

Temperatures ranged from 72 to 75 °F and humidity level 43%-53%, during the experiments. We compare ant behavior between the upper and lower segments of the same road, ensuring consistent environmental conditions. Therefore, changes within this variation of temperature will not influence the trend shown in this paper.

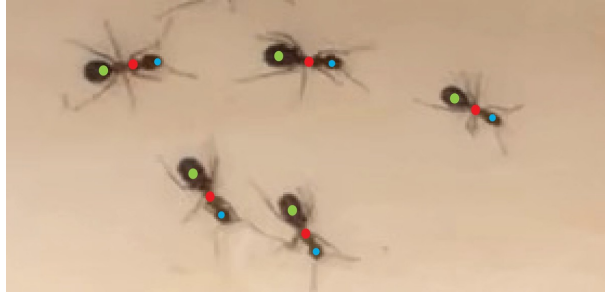


Figure 8: Annotation. Red circle: body, blue circle: head, green circle: tail

7.1.2 Annotation

For detection of each individual ant, we annotate each ant’s pose including three parts: head, body, and tail (seen in Fig. 8). We annotated 413 ants across 31 frames for training and 57 ants across 4 frames for evaluation. During annotation, the circular center of head, tail, and body parts was annotated as the center.

7.2 Video analysis and tracking

Tracking was divided into the detection stage and the tracking stage and using the working flow shown in Fig. 9 to track the ants.

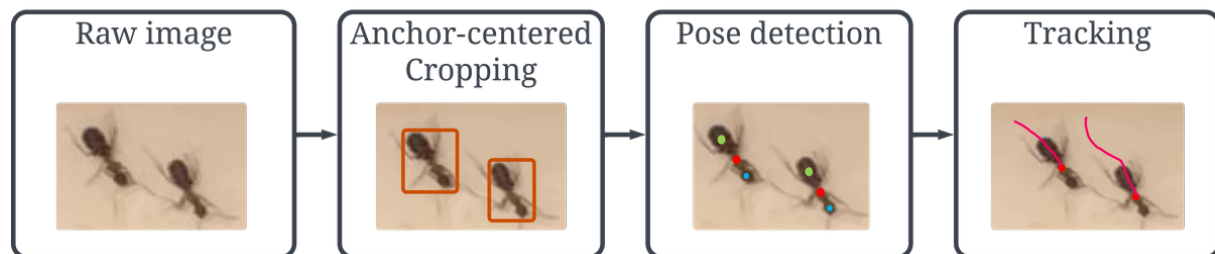


Figure 9: Ant tracking method illustration

7.2.1 Detection method

We used an anchor-based neural network with a U-Net structure (27) to detect the peak of each individual ant, then used an anchor-centered cropped around each ant. We used the cropped

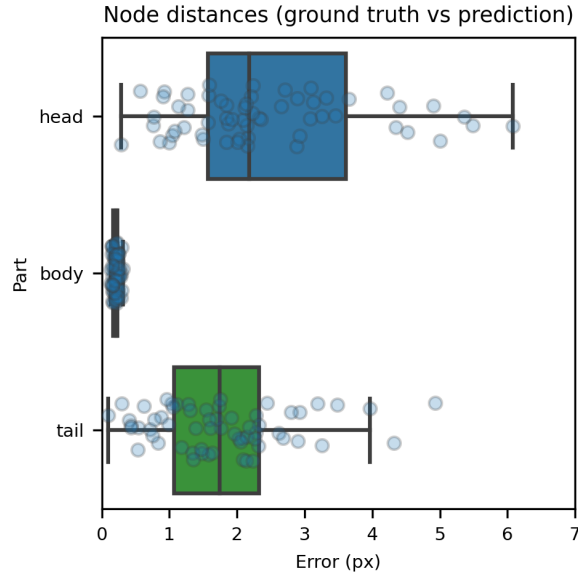


Figure 10: Detection error

image of each ant to detect the pose of each ant. The loss of training was the mean squared error of distance for each part of the pose, that is, the head, body, and tail (28). The precision of the detection of the head, body, and tail is shown in Fig. 10.

7.2.2 Tracking method

We converted the body, head, and tail to a body-centered bounding box and then calculated the similarity of the bounding box at the current frame and the predicted box of the track using previous frames. The similarity is defined as the feature distance between the detection box in the current frame and the predicted track box. We adopted an adaptive Kalman filter to predict the boundary box of the tracks. In the end, we incorporate the Hungarian Algorithm (29) to match the bounding box of this frame and previous frames based on similarity.

The MOTA (Multiple Object Tracking Accuracy) is defined as the counts of FP (false positive), FN (false negative) and id-switches (IDSW) normalized over the total number of ground



Figure 11: Tracking result demo

truth (GT) tracks.

$$r_{MOTA} = 1 - \frac{\sum_t^N (r_{FN_t} + r_{FP_t} + r_{IDSW_t})}{\sum_t^N r_{GT_t}} \quad (1)$$

The accuracy of MOTA is 90.58 %, the ID swap rate is less than 1.04%. The tracking results are illustrated in Fig. 11

7.3 Swarm tracking analysis

7.3.1 Formulation of energy for the ant

We revisit the entropy maximization formulation, as shown in Eq. 2 (30).

$$\begin{aligned} \max_{p_i} \quad & -k \sum_i^n p_i \ln p_i \\ \text{s.t.} \quad & \sum_i^n p_i = 1 \\ & \|\mathbb{E}(f(x_i)) - E\| = 0 \end{aligned} \quad (2)$$

where, $x_i \sim p_i(x_i)$. The expectation function e_i in Eq. 2 could be in a form of pressure, density, encoded features, etc. such that $E = \mathbb{E}(x_i) = kT$ can be measured. The closed form of entropy maximization seen in Eq. 3.

$$p_i = \frac{1}{E} e^{-\frac{1}{E} x_i} = \frac{1}{kT} e^{-\frac{1}{kT} x_i} \quad (3)$$

We summarize that the distribution of the speed and steering angle rate of the ants, and the energy of the physical particles are in an exponential distribution, which are the results of maximization of the entropy but with different constraints of energy (Tab. 1). Inspired by such a

distribution, our robots swarm have also adopted such distributions in experiments of moving objects and crossing each other in a narrow road.

7.4 Algorithm

7.4.1 Location algorithm

The localization of robots was defined as the heading direction of the robots and the distance towards the light source. The distance towards the light source was calculated by reading the photoresistors. The direction of light source are zero degree for each robot. To let the robot find the zero degree direction, three photoresistors were aligned with the designed angle seen in Fig. 16c such that only when l_1 and l_2 sensor sense equal value of light and l_3 sensor detects no light. The zero degree of the robot was aligned by Alg. 1.

Algorithm 1 Align angle function

```

1: function TURNTOANGLE( $\theta$ )
2:   while Turn one step to zero angle direction do
3:     if  $l_1 == l_2$  and  $l_3 = 0$  then
4:       break
5:     end if
6:   end while
7: end function

```

7.4.2 Algorithm in narrow road experiments

The robots executed Alg. 2 for narrow-road experiments both in simulation and robot experiments.

Algorithm 2 Algorithm for narrow road

```

1: while True do
2:   TurnToAngle(0) Alg. 1
3:   Sample action( $\theta_i, v_i$ ) using Eq. 4,5
4:   Robot turn to  $\theta_i$  and move with speed  $v_i$ 
5: end while

```

In the narrow road experiments, the speed was sampled using the following distribution.

$$v_i \sim p_i(v_i) = \frac{1}{kT} e^{-\frac{1}{2kT} v_i^2} \quad (4)$$

The direction of the robot was sampled by normal distribution with the norm of zero degrees for the robot moving down and 180 degrees for the robot moving up.

$$\theta_i \sim \begin{cases} N(0, 180) & \text{if } i \text{ robot goes up} \\ N(0, 180) & \text{if } i \text{ robot goes down} \end{cases} \quad (5)$$

7.4.3 Compress experiments

The robots execute Alg. 3 for experiments in narrow road in simulation.

Algorithm 3 Algorithm for compress experiments

- 1: Decide the Temperature T
 - 2: **while** True **do**
 - 3: TurnToAngle(0) Alg. 1
 - 4: Sample action(θ_i, v_i) using $p_i(v_i) = \frac{1}{kT} e^{-\frac{1}{2kT} v_i^2}$, $\theta \sim U(-180, 180)$
 - 5: Robot turn to θ_i and move with speed v_i
 - 6: **end while**
-

7.4.4 Moving object with connection

The robots executed Alg. 4 for experiments of moving object with connection in simulation.

Algorithm 4 Algorithm for moving object with connection

- 1: Decide the Temperature T
 - 2: **while** True **do**
 - 3: TurnToAngle(0) Alg. 1
 - 4: Sample action(θ_i, v_i) using $v_i \sim p_i(v_i) = \frac{1}{kT} e^{-\frac{1}{2kT} v_i^2}$, $\theta_i \sim U(-90, 90)$
 - 5: Robot turn to θ_i and move with speed v_i
 - 6: **end while**
-

Algorithm 5 Algorithm for moving object without connection

- 1: Decide the Temperature T
 - 2: **while** True **do**
 - 3: TurnToAngle(0) Alg. 1
 - 4: Sample action(θ_i, v_i) using Eq. 6,7,8
 - 5: Robot turn to θ_i and move with speed v_i
 - 6: **end while**
-

7.4.5 Moving object without connection

The robots execute Alg. 5 for experiments in narrow road in simulation. In the moving object experiments, the speed was sampled using Eq. 6.

$$v_i \sim p_i(v_i) = \frac{1}{kT_i} e^{-\frac{1}{2kT_i} v_i^2} \quad (6)$$

The temperature T_i is a function of lightness l and thread l_{thread} (Eq. 7). The steering angle of robots are uniformed sampled as Eq. 8.

$$T_i = \begin{cases} T_{liquid} & \text{if } l > l_{thread} \\ T_{gas} & \text{if } l < l_{thread} \end{cases} \quad (7)$$

$$\theta \sim U(-180, 180) \quad (8)$$

7.5 Simulation

7.5.1 Narrow road experiment

We used the ball-shaped robots in the simulation. To keep the spatial distribution of the simulation of the ants and the size of the road proportional to the biological experiments. We keep the occupation ratio the same which is defined by the area size of the ant and the area size of the road. On the road shown in Fig. 7, the ant areas without overlap can have 448 ants to cover the areas, with Ant dimension estimated as $100(\text{length of the road})/14(\text{number of ants in column})=7.14$ mm in length and around $20(\text{width of the road})/8(\text{number of ants in row}) = 2.5$ mm in width, we estimated 80 ants on average on the road giving body-to-space ratio of 0.17857.

We keep the occupation ratio (the area of the ant/area of the road) constant, which gives ball size 33mm in diameters and road length in simulation is 381.

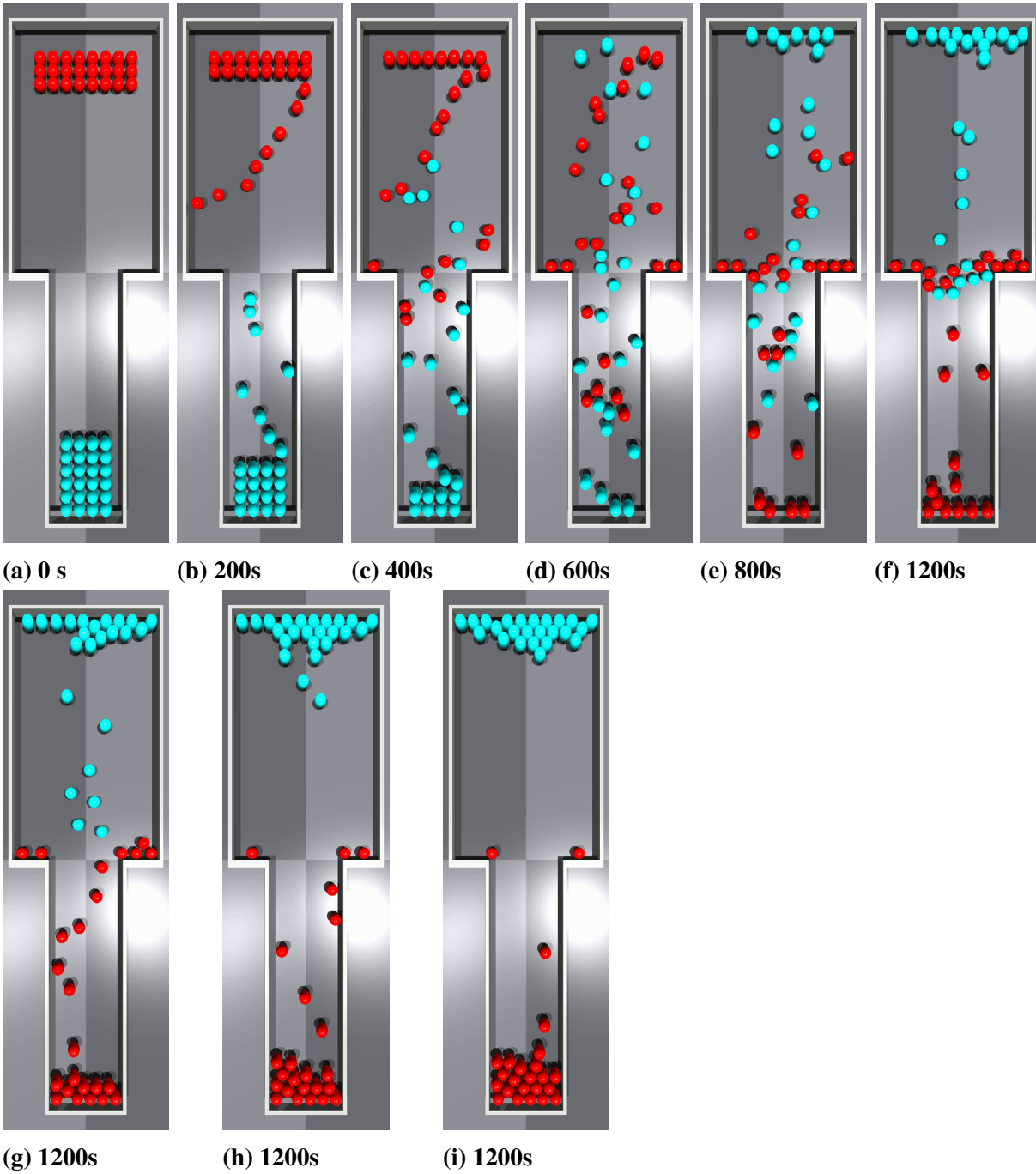


Figure 12: Robots crossing congestion

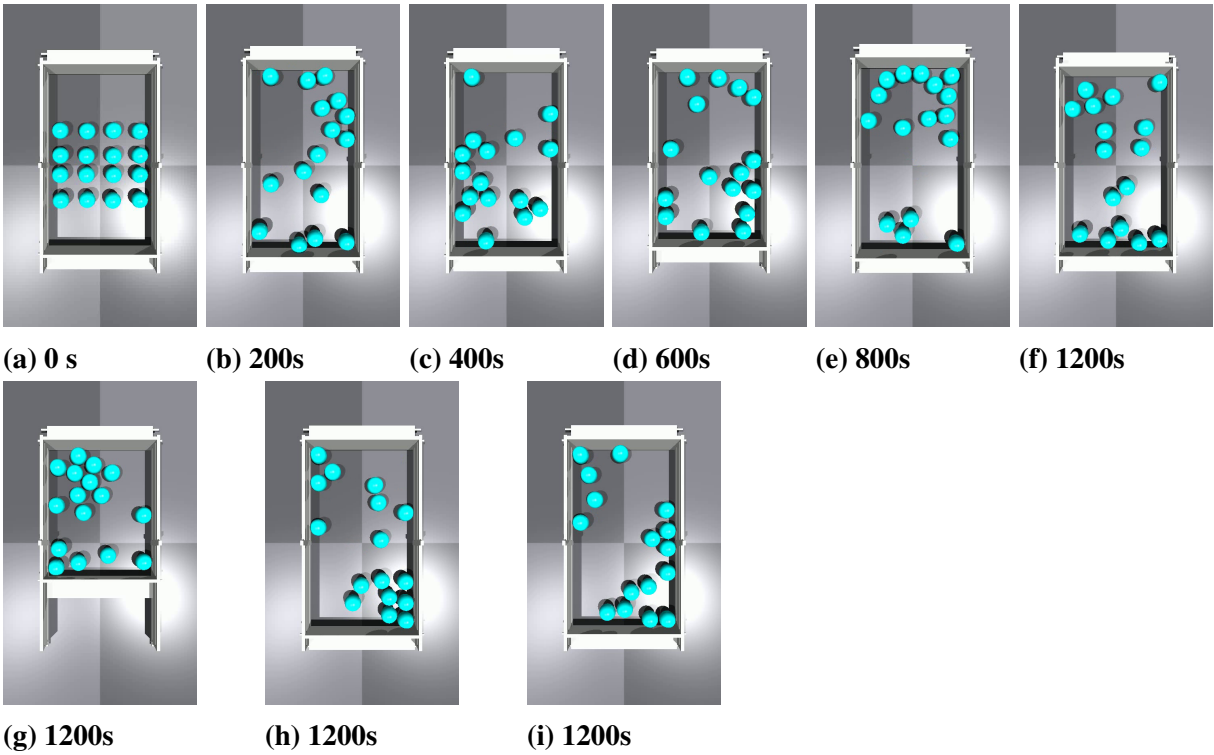


Figure 13: Compression

7.5.2 Move object with connection

The goal is to move the object to the target location which is the bottom smaller space. The robots were controlled by Alg. 4. As shown in Fig. 14, the object was moved to the target location.

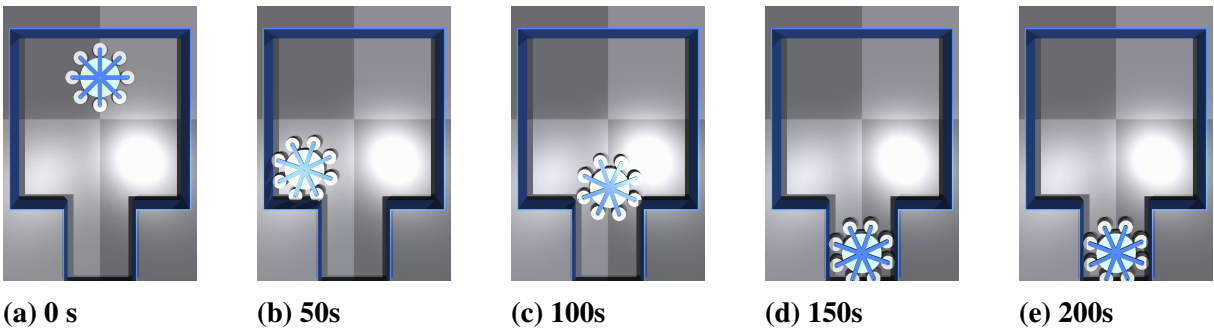
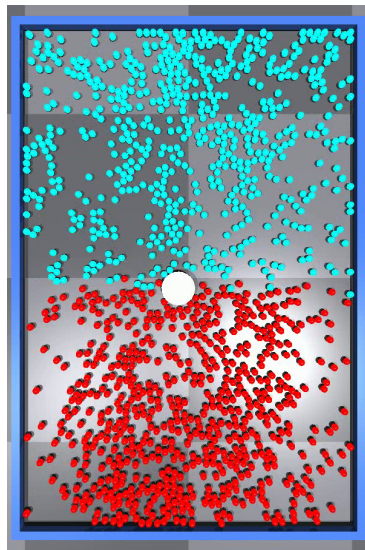


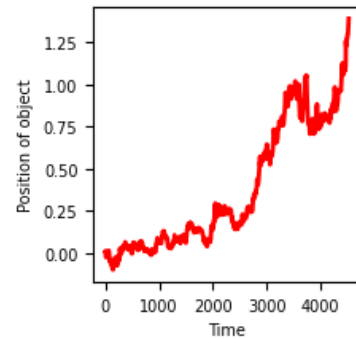
Figure 14: Robots move object without physical connection

7.5.3 Move object without connection

The goal is to move the object to the top of the constrained space. The robots in this experiment were controlled by Alg. 5. As shown in Fig. 15a, the white object was placed in the center and the goal was to move the white object from the center to the top. The vertical position of the white object was plotted in Fig. 15b.



(a) Simulation 3: move object



(b) Exp3: intelligence experiments

Figure 15: 1200 robots moving object without physical connection

7.6 Robotic experiments

7.6.1 Robots design

Each robot consists of two motors, control board, battery, gears, wheels, body, and photoresistors with an exploded view in Fig. 16c. The robot dimension is illustrated in Tab. 2 and its utilities are listed in Tab. 3. The positions of the photoresistors are illustrated in Fig. 16c.

Name	Dimension(mm)
Robot Height	60mm
Robot Diameter	33mm
Wheel diameter	12mm
Bevel gear diameter	12mm
Diameter of moving object	100mm

Table 2: Robot hardware dimension and configurations

Part name	configuration	number
Battery	Lithium Polymer Battery 3.7V 250mAh 502030	1
Motor	DC,3V,N20, 52RPM	2
Bevel Gear		2
photoresistor	GL5516 Photo Light Sensitive Resistor	3

Table 3: Robots utility configurations

7.6.2 Robot experimental settings

The configuration of the narrow road is shown in Fig. 16a. The long-duration test of robots crossing each other through a narrow road is illustrated in Fig. 4. When the robots reached the opposite end of the road, they were manually moved to the original side to test long-term operational robustness. The total duration is 1.55 hours when reaching the limit of battery storage. The dimension of experiments with moving objects is illustrated in Fig. 16b.

References and Notes

1. C. A. Yates, *et al.*, *Proceedings of the National Academy of Sciences* **106**, 5464 (2009).
2. C. Escudero, *et al.*, *Phys. Rev. E Stat. Nonlin. Soft Matter Phys.* **82**, 011926 (2010).
3. H. Shirado, N. A. Christakis, *Nature* **545**, 370 (2017).
4. O. Feinerman, I. Pinkoviezky, A. Gelblum, E. Fonio, N. S. Gov, *Nat. Phys.* **14**, 683 (2018).
5. J. Toner, Y. Tu, *Phys. Rev. Lett.* **75**, 4326 (1995).

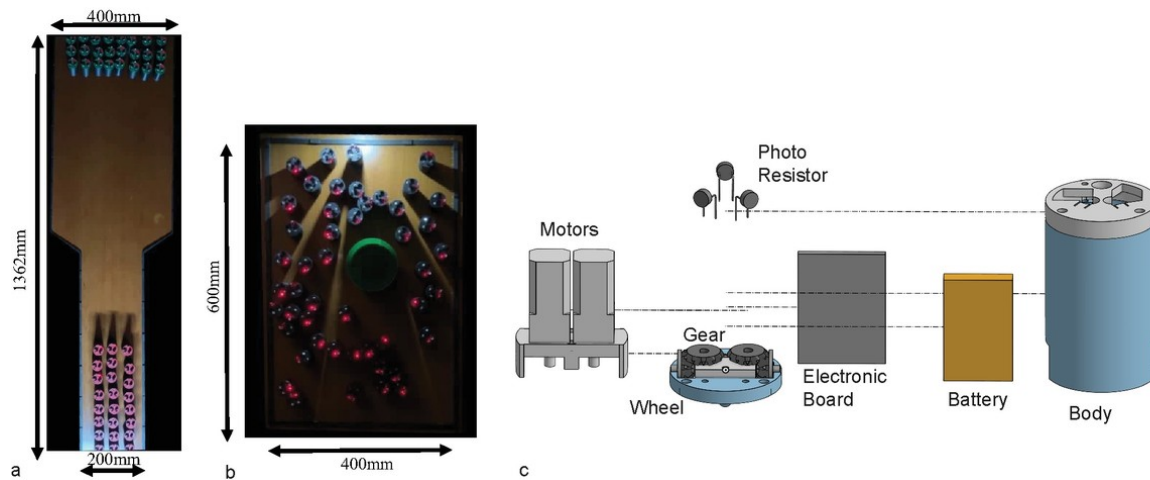


Figure 16: Robot experiments. (a) The dimension of moving object experiment. (b) The dimension of crossing experiment. (c) The exploration view of the robot hardware.

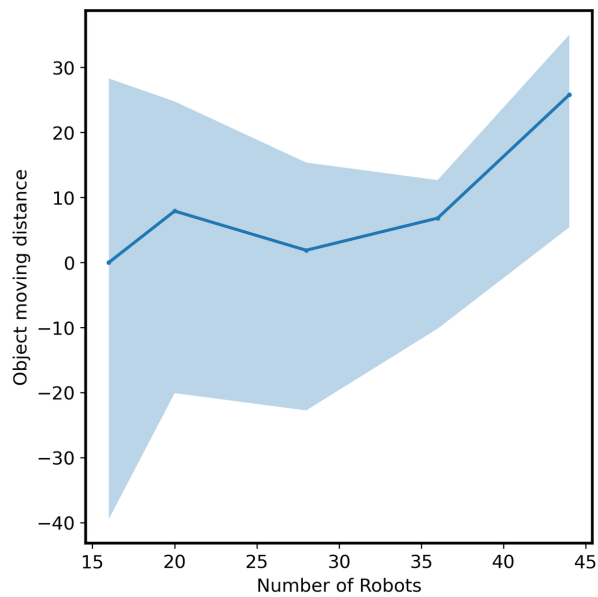


Figure 17: The moving distance of the object(positive direction is towards the lights) increases with number of robots. The variation of object movement is very high and around 0 when the number of robot is small.

6. J. Dunkel, *et al.*, *Phys. Rev. Lett.* **110**, 228102 (2013).
7. D. Helbing, I. Farkas, T. Vicsek, *Nature* **407**, 487 (2000).
8. K. Tunstrøm, *et al.*, *PLoS Comput. Biol.* **9**, e1002915 (2013).
9. R. Olfati-Saber, *IEEE Trans. Automat. Contr.* **51**, 401 (2006).
10. S. Sayin, *et al.*, *Science* **387**, 995 (2025).
11. T. Vicsek, A. Czirók, E. Ben-Jacob, I. Cohen, O. Shochet, *Physical review letters* **75**, 1226 (1995).
12. N. W. Bode, D. W. Franks, A. J. Wood, *Journal of theoretical biology* **267**, 292 (2010).
13. P. Degond, A. Frouvelle, J.-G. Liu, *Archive for Rational Mechanics and Analysis* **216**, 63 (2015).
14. D. W. Thompson, *J. Philos.* **42**, 557 (1945).
15. M. Rubenstein, A. Cornejo, R. Nagpal, *Science* **345**, 795 (2014).
16. V. Zykov, E. Mytilinaios, B. Adams, H. Lipson, *Nature* **435**, 163 (2005).
17. S. Li, *et al.*, *Nature* **567**, 361 (2019).
18. M. Yim, *et al.*, *IEEE Robot. Autom. Mag.* **14**, 43 (2007).
19. A. Spinos, D. Carroll, T. Kientz, M. Yim, *2017 IEEE/RSJ International Conference on Intelligent Robots and Systems (IROS)* (IEEE, 2017), pp. 2717–2722.
20. C. Liu, Q. Lin, H. Kim, M. Yim, *Auton. Robots* **47**, 211 (2023).
21. M. Z. Miskin, *et al.*, *Nature* **584**, 557 (2020).

22. G. Gardi, S. Ceron, W. Wang, K. Petersen, M. Sitti, *Nat. Commun.* **13**, 2239 (2022).
23. A. Kaiser, A. Snezhko, I. S. Aranson, *Sci Adv* **3**, e1601469 (2017).
24. J. Kiepenheuer, *Journal of Comparative Physiology A: Neuroethology, Sensory, Neural, and Behavioral Physiology* **57**, 409 (1968).
25. L.-A. Poissonnier, S. Motsch, J. Gautrais, J. Buhl, A. Dussutour, *Elife* **8** (2019).
26. L. Boltzmann, *Über die Beziehung zwischen dem zweiten Hauptsatze des mechanischen Wärmetheorie und der Wahrscheinlichkeitsrechnung, respective den Sätzen über das Wärmegleichgewicht* (Kk Hof-und Staatsdruckerei, 1877).
27. O. Ronneberger, P. Fischer, T. Brox, *Medical Image Computing and Computer-Assisted Intervention – MICCAI 2015*, N. Navab, J. Hornegger, W. M. Wells, A. F. Frangi, eds. (Springer International Publishing, Cham, 2015), pp. 234–241.
28. T. D. Pereira, *et al.*, *Nat. Methods* **19**, 486 (2022).
29. H. W. Kuhn, *Nav. Res. Logist. Q.* **2**, 83 (1955).
30. E. T. Jaynes, *Phys. Rev.* **108**, 171 (1957).